

Single shot quantitative and spatially resolved plasma wakefield diagnostics

Contact m.kasim1@physics.ox.ac.uk

Muhammad Firmansyah Kasim, James Holloway, Luke Ceurvorst, Matthew Levy, Naren Ratan, James Sadler, Philip N. Burrows, Peter Norreys

Clarendon Laboratory, Department of Physics, University of Oxford, Parks Road, Oxford, OX1 3PU, United Kingdom

Robert Bingham, Raoul Trines

STFC Rutherford Appleton Laboratory, Chilton, Didcot, OX11 0QX, United Kingdom

Matthew Wing

Department of Physics and Astronomy, University College London, Gower Street, London, WC1E 6BT, United Kingdom

Introduction

Plasma accelerators are getting much interest as they can provide much larger electric field than the conventional accelerators. The electric field they can produce is around 10-100 GV/m and about 3 orders of magnitude higher than the conventional accelerators [1-3]. To make a plasma accelerator, a driver (e.g. short laser pulse [4], electron beam [5], or proton beam [6]) is fired into plasma to drive a wave, which is called wakefield. The wakefield behind the driver then provides the electric field to accelerate electrons.

One main challenge in plasma wakefield experiments is inadequacy of diagnosing the plasma wakefield itself. The first technique was Frequency Domain Holography (FDH) [7]. It used a laser pulse co-propagating with the wakefield and measured the phase modulation induced by the wakefield. FDH successfully produced the snapshots of the wakefield. As the probe co-propagates with the wakefield, it integrated the wakefield density modulation along the propagation distance, and thus could not detect the evolution of the wakefield. Another recent technique is shadowgraphy [8] which fires the probe perpendicularly with the wakefield and measures the transverse profile intensity of the probe. This resulted spatially resolved plasma wakefield images, but it is hard to get the quantitative information from the results as the probe and the wakefield propagate with speed near the speed of light.

In this report, we present a technique that could diagnose the plasma wakefield in spatially-resolved and quantitative manner by probing the wakefield with some angle.

Theory

It is well known that if light propagates in medium with spatially varying refractive index, it undergoes change in wavenumber. The frequency of the light stays constant as long as the refractive index does not change in time. However, when the refractive index of the medium changes in space and time, the light experiences shifts both in wavenumber and frequency.

In plasma wakefield accelerator experiments, longitudinal waves of the plasma's electron density are driven and propagate with speed close to the speed of light. This causes the electron density in the plasma varied in space and time, thus gives the different refractive indices in different position and time.

If a laser pulse with frequency of ω_0 propagates in the plasma wakefield, part of the laser pulse gets frequency-shift, $\Delta\omega$, by the amount of [9, 10]

$$\frac{\Delta\omega}{\omega_0} \approx -\frac{\omega_p^2}{2\omega_0^2} \frac{c}{n_0} \int_{-\infty}^{\infty} \frac{\partial n}{\partial \zeta} dt \quad (1)$$

where ω_p is the plasma frequency, n and n_0 respectively denote the disturbed plasma density and initial plasma density without any disturbance. Variable $\zeta = z - ct$ is the moving longitudinal

position where z , t , and c are position and time in the lab frame and the speed of light in vacuum, respectively. By measuring the frequency change of the light, $\Delta\omega$, it is possible to obtain the modulated electron density profile, n , from equation (1).

The case considered in this report is shown in Figure 1. A driver is fired into the plasma and drives a wakefield that propagates horizontally with phase velocity of u_p . A laser probe pulse with group velocity of v_g is then fired into the wakefield with some angle, θ . Moreover, the pulse is made long enough to cover several wavelengths of the wakefield. By crossing the probe pulse with some angle, one can choose the position in the plasma to diagnose.

Assuming that the modulated electron density profile is cylindrically symmetric, the relation between pulse's frequency modulation profile and the electron density profile is as below,

$$\tilde{f}(r, k) = -\frac{1}{\pi} \int_r^{\infty} \frac{\partial \tilde{F}}{\partial y}(y, k) \frac{\cosh(ka\sqrt{y^2 - r^2})}{\sqrt{y^2 - r^2}} dy. \quad (2)$$

Here $a \equiv [(\cos\theta - u_p/v_g)/\sin\theta]$ indicates how much the light is shifted longitudinally relative to the wakefield. The electron density modulation profile as function of radius from the axis, r , and the longitudinal position of the wakefield, ζ , is represented as $f(r, \zeta) = (-\omega_p^2 c / 2\omega_0^2 n_0) (\partial n / \partial \zeta)$. The variable $F(y, \zeta_0) = (\Delta\omega / \omega_0) (v_g \sin\theta)$ represents the frequency modulation of the laser pulse as function of y and the longitudinal position of the laser, ζ_0 . The tilde hats denote the Fourier transform of the variables in ζ or ζ_0 direction. Details of the derivation of equation (2) can be found on [11].

Simulations

Three dimensional particle-in-cell (PIC) [12] simulations have been performed using OSIRIS code [13] in SCARF and ARCHER machines. The simulations were performed to model the realistic conditions expected in the experiments and to

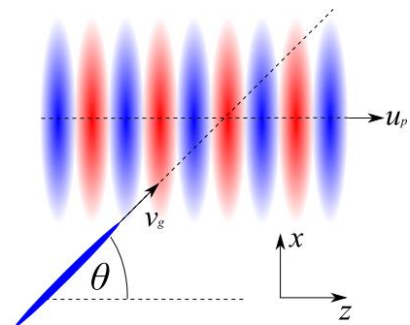


Figure 1. The case considered in this report. The y -axis is coming out of the paper and not shown in the picture.

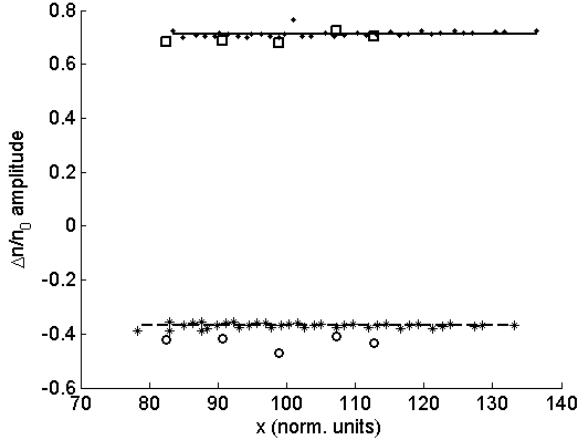


Figure 2. The comparison of peak and trough values between the measured and actual density profiles. Squares and circles are peak and trough values taken from the measured density profiles from 5 slices of the probe, while the dots and plus signs are for the actual density profiles. The solid and dashed lines are the mean values of peaks and troughs from the actual profiles.

check the accuracy of this diagnostic technique in simulations.

In the simulations, we used plasma with density of $n_0 = 2 \times 10^{19} \text{ cm}^{-3}$. For the driver, we employed a short electron beam which had a spherical Gaussian density profile with $\sigma_r = 4.4 \mu\text{m}$, peak density of $n_e = 0.33n_0$, and momentum of $p/m_e c = 45 \times 10^3$, where m_e is the mass of electron. As a probe, a plane wave with wavelength of 400 nm, duration of 53 fs, and normalized intensity of $a_0 = 0.01$ is employed. The probe pulse crosses the wakefield with angle of $\theta = 20^\circ$. Slices of the probe pulse which crosses the wakefield at $s = 28, 39, 49, 60$, and $67 \mu\text{m}$ after entering the plasma were taken to obtain the frequency modulation profile of the slices.

The frequency modulation profiles obtained from the slices then were inserted into equation (2) to get the measured electron density profiles at the crossing points. These profiles were then compared to the density profiles obtained directly from the simulation. The former density profiles are called “measured” profiles, while the latter profiles are called “actual” profiles.

Besides doing simulations for the baseline parameters, we also performed parameters scanning. The peak density of the driver beam was varied from $0.1n_0$ to $0.35n_0$, the angle from 25° down to 5° , and the probe’s wavelength from 260 to 800 nm. The actual and measured density profiles are then compared to see the accuracy of the diagnostics.

Results

For each simulation, the peak and trough values of the density modulation profiles were obtained. The comparison between peak and trough values of the measured and the actual density profiles for the baseline parameters is shown in Figure 2. The graph shows the peak and trough values from the measured and actual density profiles agree quite well.

The next comparison was done by taking the mean value of amplitudes for various positions in the actual and measured profiles. The relative errors between the average values from those profiles are calculated to see the accuracy of the measurement. The amplitude is defined here as half of difference between the peak and trough values.

First, the peak density of the electron driver was varied from $0.1n_0$ to $0.35n_0$ while keeping the other parameters same as the baseline parameters. This was to cover the linear and non-linear regime of the wakefield where the wakefield amplitude varied between $\sim 0.03n_0$ and $\sim 0.6n_0$. The actual and measured

amplitude values as well as the relative errors are shown in Figure 3 (a) and (b), respectively. Here it can be seen that no relative error exceeds 10%.

The next comparison was done by varying the probe’s frequency from $9.8\omega_p$ to $30\omega_p$ for crossing angle of 20° and 15° . The amplitude values and their relative errors are shown in Figure 3 (c)-(d). The figures show that none of the relative errors for the tested case higher than 15% while most of them are less than 10%.

Besides varying the amplitude of the driver and the probe’s frequency, the crossing angle was also varied between 5° and 25° . The comparison results are shown in Figure 3 (e)-(f). In this case, the relative errors are still below 10% for $\theta > 10^\circ$. However, the relative errors increase much when the crossing angle gets smaller. This could happen because of diffraction.

As the crossing angle is getting smaller, the interaction length between the probe and the wakefield is getting longer. If the probe pulse already diffracts while it is still interacting with the wakefield, the frequency modulation of the probe pulse gets smaller than it should be. In order to avoid this effect, the crossing angle should be large enough, or

$$\sin \theta > \frac{\lambda_0}{\sqrt{\pi} r_p} \quad (3)$$

where λ_0 is the probe’s wavelength and r_p is the wakefield’s radius.

Conclusion

We have developed a mathematical transformation and its inverse for the measurement of cylindrically symmetric wakefield density profile with non-perpendicular laser pulse using photon acceleration. The transformation can also be applied for more general case that involves cylindrically symmetric object with non-perpendicular probe.

To check the accuracy of the diagnostic technique, 3D PIC simulations were performed for various wakefield amplitudes, crossing angles, and the probe’s frequencies. Most of the simulated cases show the relative errors of the simulated measurements do not exceed 10%, except for the small crossing angle where the diffraction gets more significant. By considering the constraints in this diagnostic technique, it is possible to diagnose the plasma wakefield’s electron density profile at a chosen point in the plasma.

Acknowledgements

The authors would like to acknowledge the support from the plasma physics HEC Consortium EPSRC Grant No. EP/L000237/1, as well as the Central Laser Facility and the Scientific Computing Department at the Rutherford Appleton Laboratory for the use of SCARF-LEXICON computer cluster. We would also like to thank ARCHER UK National Supercomputing Service for the use of the computing service. We also wish to thank the UCLA/IST OSIRIS consortium for the use of OSIRIS and also to the Science and Technology Facilities Council for its support to AWAKE-UK (Grants No. ST/K002244/1 and No. ST/M007375/1). One of the authors (M. F. Kasim) would like to thank Indonesian Endowment Fund for Education for its support. M. C. L. thanks the Royal Society Newton International Fellowship for support. J. S. and N. R. acknowledge the support from Engineering and Physical Sciences Research Council. M. W. acknowledges the support of DESY, Hamburg, and the Alexander von Humboldt Foundation. The work is part of EuCARD-2, partly funded by the European Commission, GA 312453. The authors gratefully acknowledge the support of all of the staff of STFC’s Central Laser Facility in the execution of this work.

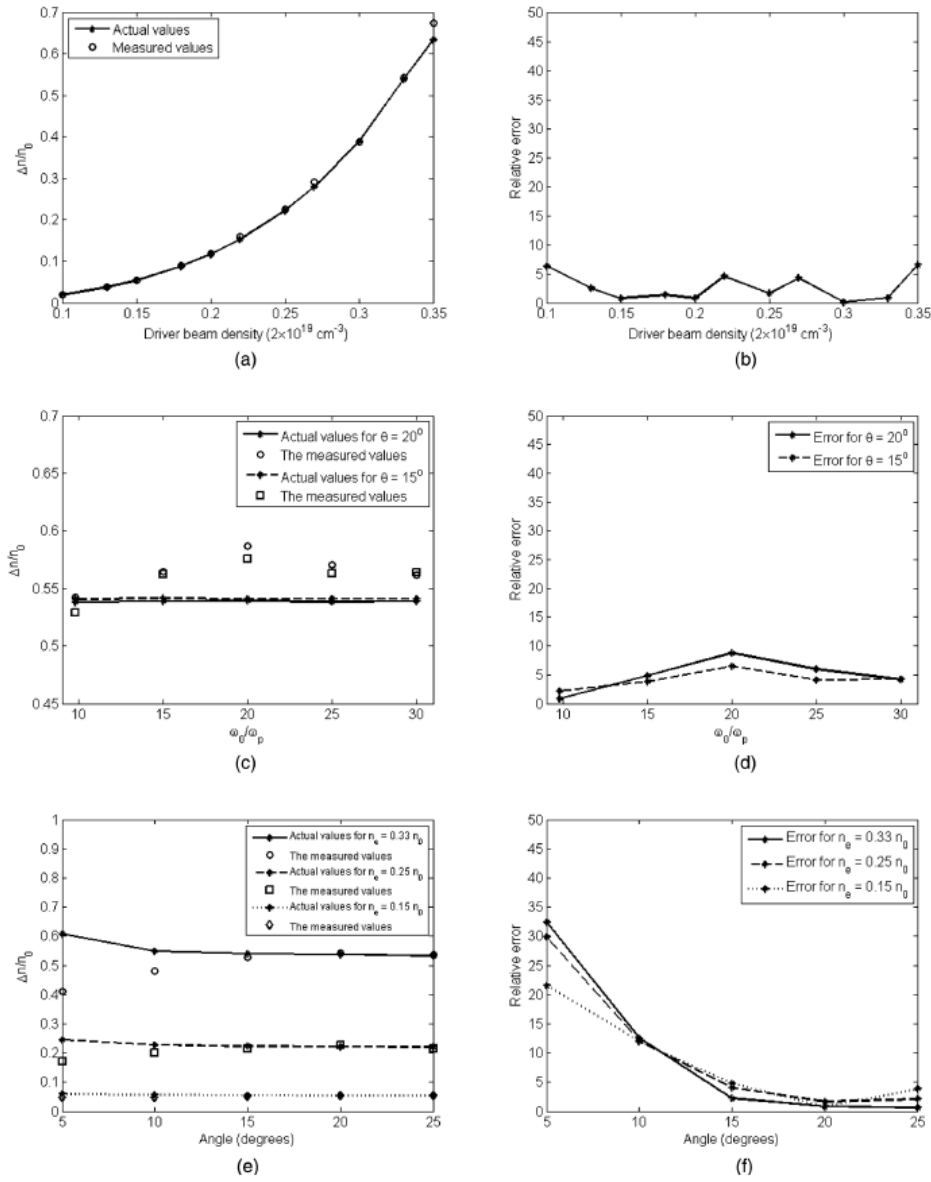


Figure 3. Comparison of the amplitude values between the measured and actual density profiles for (a) various peak driver beam density values and (b) the relative errors, (c) various probe's frequencies and (d) its relative errors, and (e) various crossing angles with (f) its relative errors.

References

1. S. P. D. Mangles, C. D. Murphy, Z. Najmudin, A. G. R. Thomas, J. L. Collier, A. E. Dangor, E. J. Divall, P. S. Foster, J. G. Gallacher, C. J. Hooker, *et al.*, *Nature* **431**, 535 (2004).
2. J. Faure, Y. Glinec, A. Pukhov, S. Kiselev, S. Gordienko, E. Lefebvre, J.-P. Rousseau, F. Burgy, and V. Malka, *Nature* **431**, 541 (2004).
3. C. G. R. Geddes, Cs. Tòth, J. van Tilborg, E. Esarey, C. B. Schroeder, D. Bruhwiler, C. Nieter, J. Cary, and W. P. Leemans, *Nature* **431**, 538 (2004).
4. V. Malka, S. Fritzler, E. Lefebvre, M.-M. Leonard, F. Burgy, J.-P. Chambaret, J.-F. Chemin, K. Krushelnick, G. Malka, S. P. D. Mangles *et al.*, *Science* **298**, 1596 (2002).
5. M. Litos, E. Adli, W. An, C. I. Clarke, C. E. Clayton, S. Corde, J. P. Delahaye, R. J. England, A. S. Fisher, J. Frederico *et al.*, *Nature* **515**, 92-95 (2014).
6. A. Caldwell, K. Lotov, A. Pukhov, and F. Simon, *Nat. Phys.* **5**, 363 (2009).
7. N. H. Matlis, S. Reed, S. S. Bulanov, V. Chvykov, G. Kalintchenko, T. Matsuoka, P. Rousseau, V. Yanovsky, A. Maximchuk, S. Kalmykov, *et al.*, *Nature Phys.* **2**, 749 (2006).
8. A. Sävert, S. P. D. Mangles, M. Schnell, J. M. Cole, M. Nicolai, M. Reuter, M. B. Schwab, M. Möller, K. Poder, O. Jäckel, *et al.*, arXiv:1402.3052 (2014).
9. S. C. Wilks, J. M. Dawson, W. B. Mori, T. Katsouleas, and M. E. Jones, *Phys. Rev. Lett.* **62**, 2600 (1989).
10. J. M. Dias, L. O. Silva, and J. T. Mendonça, *Phys. Rev. ST Accel. Beams* **1**, 031301 (1999).
11. M. F. Kasim, J. Holloway, L. Ceurvorst, M. C. Levy, N. Ratan, J. Sadler, R. Bingham, P. N. Burrows, R. Trines, M. Wing, and P. Norreys, *Phys. Rev. ST Accel. Beams* **18**, 081302 (2015).
12. C. K. Birdsall and A. B. Langdon, *Plasma Physics via Computer Simulation* (CRC Press, 2004).
13. R. A. Fonseca, L. O. Silva, F. S. Tsung, V. K. Decyk, W. Lu, C. Ren, W. B. Mori, S. Deng, S. Lee, T. Katsouleas, *et al.*, *Lecture Notes in Computer Science* Vol. 2329, III-342 (Springer, Heidelberg, 2002).